Frequency-Domain Methodology for Measuring MIMO Channels Using a Generic Test Bed

Jesús Gutiérrez, *Student Member, IEEE*, Óscar González, *Student Member, IEEE*, Jesús Pérez, *Member, IEEE*, David Ramírez, *Student Member, IEEE*, Luis Vielva, Jesús Ibáñez, *Member, IEEE*, and Ignacio Santamaría, *Senior Member, IEEE*

***Abstract*—A multiple-input multiple-output (MIMO) frequency-domain channel measurement methodology is presented. This methodology can be implemented in any transmit/receive hardware consisting of radio frequency modules and baseband digital processing units. It involves the transmission and reception of frequency and phase-optimized complex exponentials through antenna arrays, followed by an offline frequency estimation, which makes additional synchronization circuitry unnecesary. To test the feasibility of this method, a series of measurements is presented, employing a 4 × 4 dual-band (2.4/5 GHz) MIMO test bed.**

***Index Terms*—Estimation, frequency estimation, MIMO systems, multipath channels, signal detection, signal processing, spectral analysis.**

I. Introduction

THE DEMAND for capacity in wireless communications has given rise to much research on multiple-input multiple-output (MIMO) systems. The adoption of MIMO technologies for the air interface of new wireless communication systems promises to meet the increasing data rate demands of future applications. Since the pioneering work of Foschini and Gans [1] and Telatar [2], multiple antennas have been used to drastically improve the performance of wireless communication systems. This is particularly important in systems where the capacity achieved with traditional techniques is limited due to the adverse characteristics of the propagation environment.

The propagation scenario in a wireless communication system is very complex, and the signal transmitted from an antenna will reach the receiving antenna as multiple versions caused by objects in the environment. These are received with different time delays and are collectively referred to as multipath. The characteristic of indoor multipath propagation [3] and its impact on the performance of MIMO systems have been of continued interest, particularly for the design and evaluation of MIMO wireless local area network (WLAN) systems. As an example, different MIMO channel models have been produced [4]–[7] for different environments. However, numerous MIMO techniques have not been sufficiently tested under realistic propagation conditions yet, and hence, their integration into real applications still requires further experimental work. This fact underlines the importance of developing methods to understand and characterize the wireless channel.

MIMO channel sounding techniques [8] can be classified in accordance with two criteria: the excitation signals that determine the characterization domain (time or frequency) and the multiplexing technique that allows for transmitter antenna identification. Different kinds of measurement signals can be used for channel sounding, and these signals can be categorized by pulse-shaped or continuous-wave (CW) signals and by narrowband or wideband signals. Regarding the transmit antenna identification, there exist three multiplexing techniques [9]: time-division multiplexing (TDM), frequency-division multiplexing (FDM), and code-division multiplexing (CDM). The choice of which multiplexing technique is used is partially constrained by the feasibility of constructing the hardware, as well as the desired resolution of the channel measurements.

Our interest centers on measuring the MIMO channels in the frequency domain. For this purpose, a methodology has been designed involving the transmission of a set of frequency and phase-optimized complex exponentials within the bandwidth of interest, the subsequent acquisition through the receive antennas, and the offline execution of frequency estimation algorithms. In the final stage, the amplitude, phase, and frequency of the received exponentials are estimated by means of a high-accuracy nonparametric frequency estimation method based on the fast Fourier transform (FFT), which is referred to as the iterative weighted phase averager (IWPA) [10] algorithm. The use of this algorithm avoids the need of additional circuitry or cables to synchronize the transmitter and receiver setup. Moreover, the methodology does not require the real-time signal processing provided by field-programmable gate arrays (FPGAs) or digital signal processors. These simplifications do not avoid a thorough calibration at both the transmitter and receiver sides.

To perform the MIMO channel measurements, there exists dedicated hardware, such as channel sounders [11]–[13] or vector network analyzers [14], [15]. The proposed channel characterization methodology, however, can be implemented in any

Manuscript received December 27, 2009; revised June 22, 2010; accepted June 23, 2010. Date of current version February 9, 2011. This work was supported by the Spanish Ministry of Education and Science under FPU Grant AP2006-2965, under FPI Grant BES-2008-002085, through the MIMO Technologies for Multiterminal Wireless Networks (MultiMIMO) Project under Grants TEC2007-68020-C04-02/TCM and TEC2008-00924-E/TEC, and through the Advanced MIMO Systems for Maximum Reliability and Performance (MIMAX) Project. The Associate Editor coordinating the review process for this paper was Dr. Rik Pintelon.

The authors are with the Department of Communications Engineering, University of Cantabria, 39005 Santander, Spain (e-mail: jesusgt@gtas.dicom.unican.es; oscargf@gtas.dicom.unican.es; jperez@gtas.dicom.unican.es; ramirezgd@gtas.dicom.unican.es; luis@gtas.dicom.unican.es; jesus@gtas.dicom.unican.es; nacho@gtas.dicom.unican.es).

Color versions of one or more of the figures in this paper are available online at http://ieeexplore.ieee.org.

Digital Object Identifier 10.1109/TIM.2010.2082432

transmit/receive hardware consisting of radio frequency (RF) modules and baseband (BB) digital processing units (DPUs), thus providing great flexibility. A dual-band (2.4/5 GHz) MIMO test bed has been used in order to perform the channel measurements. These test beds [16]–[18] allow wireless transmissions, online processing (FPGA), and data storage.

This paper is organized as follows. An introduction and background on channel sounding is briefly presented in Section II. The main features of the developed methodology are explained in Section III, including the generation of the complex exponentials at the transmitter along with a brief review of the estimation algorithm (see Section III-A2) implemented at the receiver. Section IV presents the 4×4 flexible MIMO test bed used to test the methodology and to carry out the measurements. In Section V, the indoor propagation scenario is described, and the experimental results are presented. Finally, the obtained conclusions are put forward in Section VI.

II. Background on Radio Channel Sounding

Channel sounders provide the temporal and spatial characteristics of the MIMO channel with an accuracy and a resolution that are high enough to befit the design purpose. This is completely determined by channel sounding features, such as the excitation signals to be considered (see Section II-A) and the multiplexing strategies to be implemented (see Section II-B).

A. Excitation Signals

The excitation signal choice is a key aspect in channel sounding since it determines the following signal processing to be applied and has implications on the hardware.

The first sounding experiments have been carried out by using single-tone CW signals. This was sufficient as long as only the narrow-band channel behavior was of interest. In order to achieve a high delay resolution, sequential sounding [19] at a number of different frequencies was developed. Its drawback is the resulting huge measurement time, which is not suitable for high-mobility measurements.

The pulse compression approach is well known from the spread spectrum technology and makes these signals very useful for the real-time identification of time-delay systems since all frequencies are instantaneously excited and a considerable SNR processing gain is achieved in the time domain by correlation. Examples of these excitation signals are the periodic pseudorandom binary signals (PRBSs) [20] or the pseudorandom noise signals [12], [21]. They can be generated easily, and they serve as broadband excitation signals. This is applied in the classical swept time-delay cross-correlation sounder implementation [22]. The disadvantage of this principle, working sequentially, is again the long measurement time which prohibits real-time operations. Pulse compression using the chirp technique [23]–[25] has proven to be a powerful method for measuring the channel response since it avoids transmitter peak power limitations and offers excellent interference rejection capabilities. In general, the application of chirp signals for mobile radio channel characterization has always been limited by the capabilities of modern digital technology.

Finally, a flexible concept of excitation signals for measuring the channel frequency response includes multifrequency signals [9], [26]–[28]. This approach is well known from the frequency-domain system identification in measurement engineering. The advantage of this kind of signals is that the channel frequency response can be measured at desired frequencies. These signals present high peak-to-average power ratio (PAPR) levels which can be reduced by numerical optimization. The difference, in comparison to the PRBS, is that the phases and magnitudes of the Fourier coefficients can be arbitrarily chosen in order to optimize the system performance.

B. Multiplexing Techniques

The resolution and capability of a channel sounder are determined by the choice of the hardware architecture and multiplexing strategy. There are three multiplexing schemes for MIMO channel sounders: TDM, CDM, and FDM.

The aim of the MIMO sequential channel sounding (TDM) is to distinguish the transmit antennas as well as to reduce the complexity and the cost. Multiple sequentially switched antenna arrays at both ends, denoted as fully switched systems [12], [28], make use of a multiplexing unit that is used to step a single RF chain through all transmit/receive antenna elements sequentially in time. In a semiswitched system [21], [25], [29], the receivers operate in parallel, whereas a switching scheme is implemented at the transmitter. The use of parallel receive channels allows the high-resolution measurements of the radio environment without further reducing the effective sampling rate of the channel. This scheme is not suitable for real-time channel measurement and has some major drawbacks, such as the requirement of precise synchronization between the transmitter and the receiver and accuracy reduction during switching time.

Switching can be avoided using parallel transmitters and parallel receivers [30]. Clearly, the more elements that are used, the greater the requirement for using parallelism within the system. Moreover, the snapshot time (i.e., the time over all temporal multiplexed channels) is significantly reduced if we compare with a fully switched scheme. This approach supports FDM and CDM, each with different advantages/drawbacks. With the FDM, a subset of the spanned frequencies is assigned to each antenna; thus, they do not all characterize the channel at exactly the same frequencies. The CDM will give excellent discrimination between antenna elements, provided that a low correlation between the codes is maintained within the channel being sounded. Unfortunately, as the channel is a multipath one, the cross correlation between the codes at nonzero delays is important.

III. Proposed Methodology

The proposed methodology has been divided into two different parts. The first one involves measuring single-input multiple-output (SIMO) channels, which is presented in Section III-A. It comprises the generation of the excitation signals as well as the offline estimation technique. The second one extends the method to a MIMO scheme, and it is summarized in Section III-B by implementing a

switching-in-time transmission that allows transmitter identification at the receiver side.

The proposed methodology, presented in a general way, can be implemented in any transmit/receive hardware consisting of RF modules and BB DPUs.

A. SIMO Channel Measurement Procedure

To measure SIMO channels, first, it is necessary to generate a robust signal with the objective of mitigating common issues, such as local oscillator (LO) leakage, inphase and quadrature (IQ) imbalance, and frequency offset. The signal generation and its optimization are presented in Section III-A1. After that, the received signal is stored and processed at the receiver, applying the algorithm described in Section III-A2. This algorithm is a high-accuracy estimation technique of the frequency, amplitude, and phase, based on the FFT denoted as the IWPA [10].

1) Signal Generation at the Transmitter Side: Among the feasible excitation signals to transmit in order to carry out the frequency channel estimation, multifrequency probing signals have been chosen due to their spectral flexibility. The following lines describe the signal design in detail as well as the necessary steps to choose the right excitation parameters, focusing on the minimization of hardware effects.

Defining $s[n]$ as a discrete signal of samples with length N which consists of M complex exponentials placed at certain equally spaced frequencies f_i

$$s[n] = \sum_{i=1}^{M} A_i e^{j(\omega_i n + \phi_i)} \qquad n = 0, \ldots, N \tag{1}$$

where ϕ_i denotes the chosen phases in order to solve the PAPR issue (see Section III-A1b), A_i denotes the resulting amplitudes obtained in the calibration process (see Section III-A1c), and ω_i denotes the frequencies of the discrete-time complex exponentials

$$\omega_i = \frac{2\pi f_i}{f_s} \tag{2}$$

where f_s is the sampling frequency.

On the other hand, the frequency-domain representation of $s[n]$, i.e., the output of the N_{FFT}-point discrete Fourier transform (DFT), can be written as

$$S[k] = A[k] e^{j\phi[k]} \qquad k = \left[-\frac{N_{\mathrm{FFT}}}{2}, \ldots, \frac{N_{\mathrm{FFT}}}{2} - 1 \right]. \tag{3}$$

Regarding the methodology proposed in this paper, whose processing is based on the DFT and is intended to be performed over a large variety of devices, we impose several constraints.

Constraint 1: The exponentials' frequencies must be lined up with DFT sampling, i.e., $k_i = (\omega_i N_{\mathrm{FFT}}/2\pi)$, in order to make them orthogonal. That is

$$S[k] = \begin{cases} A_i e^{j\phi_i}, & \text{if } k = k_i \\ 0, & \text{otherwise.} \end{cases} \tag{4}$$

Constraint 2: To ensure an equispaced channel excitation, the same separation among exponentials $\Delta w_i = \text{constant}$ is chosen. In terms of used DFT bin spacing Δk_i, this can be summarized as

$$\Delta k_i = \text{constant}, \qquad \forall\, i. \tag{5}$$

Constraint 3: In order to avoid the presence of the LO leakage, we impose that

$$S[0] = 0. \tag{6}$$

Constraint 4: Finally, the phase and amplitude imbalances existing in the IQ modulator aside from the IQ branch imbalances introduced by filtering, amplifications, and D/A and A/D conversions are considered as an effect called the IQ imbalance. It can be characterized by two parameters: the amplitude imbalance (ΔG) between the I and Q branches and the phase orthogonality mismatch (ΔP). We denote $s'[n]$ as the signal $s[n]$ when it is affected by IQ imbalance, which can be written [31] as

$$s'[n] = \alpha s[n] + j\beta s^*[n] \tag{7}$$

where * denotes the complex conjugate

$$\alpha = \cos\Delta P + j\Delta G \sin\Delta P \tag{8}$$
$$\beta = \Delta G \cos\Delta P - j \sin\Delta P. \tag{9}$$

Thus, the IQ imbalance frequency-domain effect

$$S'[k] = \alpha S[k] + j\beta S^*[-k] \tag{10}$$

consists in a mirror frequency regrowth, producing crosstalk between symmetrical exponential pairs (regarding the LO frequency). A simple solution in order to avoid this issue is shifting the whole spectrum one DFT bin around the RF in such a way that

$$S[k] \neq 0 \Leftrightarrow S[-k] = 0. \tag{11}$$

It is obvious that, according to Constraints 1–4, the separation between the used DFT bins must be an integer value fulfilling

$$\Delta k_i \in \left[3, \frac{N_{\mathrm{FFT}} - 1}{M} \right]. \tag{12}$$

Furthermore, these constraints and other parameters, such as the desired bandwidth to be measured BW and the frequency resolution Δf, determine the number of exponentials M and frequencies f_i to be chosen. The procedure, which has been developed to obtain these parameters, is presented in Section III-A1a. As a drawback, this kind of multifrequency signals also leads to a large PAPR, so aiming at its reduction, the search of the optimal phases ϕ_i is performed by an algorithm described in Section III-A1b. The amplitudes of the resulting exponentials A_i must be calibrated (see Section III-A1c) to get a flat frequency response.

a) Calculation of the number of exponentials (M) and frequencies (f_i): Two key design parameters of a frequency-domain channel measurement system are the bandwidth of interest BW and the frequency resolution Δf. Furthermore,

Input: BW, Δf, f_s, N_{FFT}

Output: M, $\{f_i\}$

$$M = \left\lfloor \frac{BW}{\Delta f} \right\rfloor$$

$$\Delta k_{min} = 3, \qquad \Delta k_{max} = \left\lfloor \frac{N_{FFT}}{M} \right\rfloor$$

$$\Delta k' = \underset{\Delta k_{min} \le \Delta k \le \Delta k_{max}}{\arg\min} \left| \frac{\Delta k}{N_{FFT}} \cdot f_s - \Delta f \right|$$

for $i = -\left\lfloor \frac{M}{2} \right\rfloor$ **to** $\left\lfloor \frac{M}{2} - 1 \right\rfloor$ **do**

$$k_i = 1 + \Delta k'$$

$$f_i = k_i \frac{f_s}{N_{FFT}}$$

end

Algorithm 1: Developed procedure to obtain the number of exponentials M and their frequencies f_i.

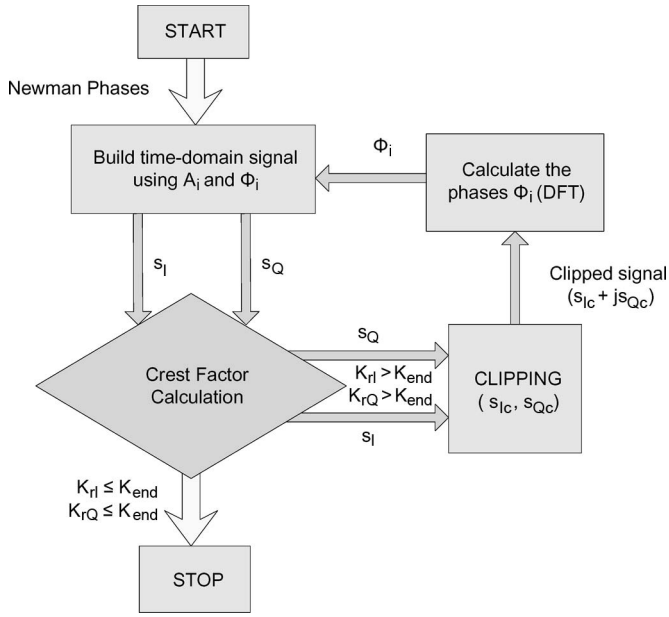

Fig. 1. Block diagram of the crest factor calculation.

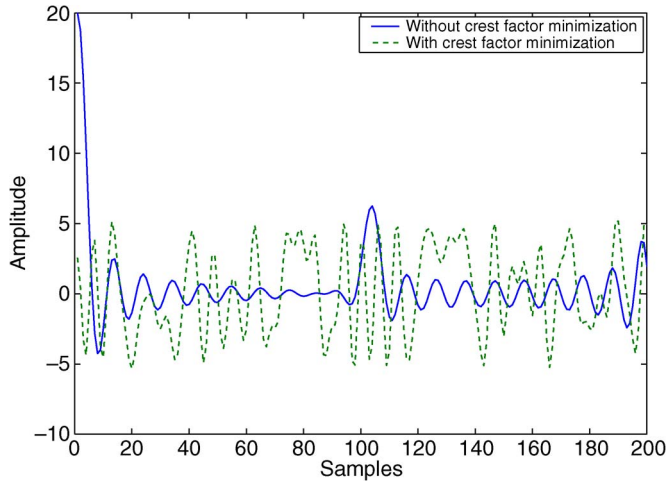

Fig. 2. Comparison of the transmitted signal before and after crest factor correction.

other common limitations that come up from the hardware include a predefined set of sampling frequencies f_s and a limited processing power (i.e., the maximum affordable length of the DFT) N_{FFT}.

Subsequently, Algorithm 1, which calculates M and f_i by considering BW, Δf, f_s, and N_{FFT} as input parameters, is described. This algorithm strictly fulfills the hard constraints imposed in Section III-A1 while trying to fit the soft constraints pointed out as input parameters.

b) Phase (ϕ_i) calculation: The choice of the proper signal phases tries to avoid an inefficient use of the dynamic range of the electronic devices due to a high PAPR. The power peaks derived from the phase alignments may cause nonlinear effects, giving rise to intermodulation products that can distort other exponentials. Low PAPR signals are distinguished by a flat time-domain envelope.

This phase optimization has been carried out by modifying a minimization algorithm [32] that relies on a mixture of clipping and phasing strategies. The goal of this modification is to simultaneously minimize the crest factor (the square root of the PAPR) of the $s[n]$ real and imaginary parts.

Therefore, considering the discrete signal $s[n] = s_I[n] + js_Q[n]$ of length N and denoting the peak-to-peak amplitude of the real and imaginary parts as $s_{I_{\mathrm{pp}}}$ and $s_{Q_{\mathrm{pp}}}$, respectively, we have the following definitions for the real and imaginary crest factors:

$$K_{r_I} = \frac{s_{I_{\mathrm{pp}}}/2}{2\sqrt{\frac{1}{N}\sum_{n=0}^{N-1} s_I[n]^2}} \qquad K_{r_Q} = \frac{s_{Q_{\mathrm{pp}}}/2}{2\sqrt{\frac{1}{N}\sum_{n=0}^{N-1} s_Q[n]^2}}. \tag{13}$$

Several closed-form expressions have been proposed to obtain the suboptimal phases for multifrequency signals. Newman phases [33] will serve as the starting point on our phase optimization procedure, which is depicted in Fig. 1. The assigned phases to the ith complex exponential (for both real and imaginary parts) are

$$\phi_i = \pi \cdot \frac{(i-1)^2}{M}, \qquad 1 \le i \le M. \tag{14}$$

First, the time-domain signal $s[n]$ is built with the initial amplitudes and the Newman phases. Then, the crest factor calculation is performed. The real (s_I) and imaginary (s_Q) components are clipped (s_{I_c} and s_{Q_c}, respectively) in the time domain to cut off the peaks. Subsequently, they are combined, and the DFT is performed to obtain the new phases ϕ_i. This procedure is cyclically repeated until both the real and imaginary crest factors are lower than a threshold ($K_{r_I} < K_{\mathrm{end}}$ and $K_{r_Q} < K_{\mathrm{end}}$). With a few iterations, a quasi-optimal solution (a multifrequency signal with a constant envelope around $\sqrt{M}$) is obtained for signals with the same amplitude. This fact is noticeable in Fig. 2.

c) Amplitude (A_i) calculation: To separate the actual channel response from the circuitry effects, a back-to-back system calibration procedure must be performed by means of a cable connecting in pairs every transmit-and-receive antenna. This aims at ensuring that the transmitter and receiver frequency responses, as well as the power amplifier nonlinearities, are removed from the measured data. As a result, a set of M amplitude coefficients A_i is obtained, being applied to each exponential in order to compensate for the circuitry response.

It must be noticed that modifying the amplitude of the exponential affects the PAPR optimization performed in Section III-A1B. Therefore, it can be necessary to iteratively recalculate the optimal phases and amplitudes if optimal results are desired.

2) Signal Processing at the Receiver Side (IWPA): Since we do not intend to perform a physical synchronization by means of cables or additional hardware, the signal processing at the receiver side must handle this issue in order to ensure a proper synchronization. An algorithm able to deal with this problem has been used.

This algorithm, denoted as the IWPA [10], is a high-accuracy nonparametric frequency estimation method based on the FFT. It is able to provide accurate frequency estimates even when the signals are not well separated in frequency (even with less than $1/T$, where T is the observation time of the signal). It has been modified in order to deal with complex exponentials instead of sinusoids. This method is able to reduce both the short- and long-range spectral leakage. The received signals can be expressed as

$$r[n] = \sum_{i=1}^{N} A_i' \cdot e^{j\left(\omega_i' n + \phi_i'\right)} + w[n]. \tag{15}$$

First, the FFT is performed to obtain the spectrum. The frequency of the received complex exponential $\hat{f}_i'$ is estimated as the frequency corresponding to the largest FFT output coefficient magnitude (coarse estimation) and a frequency interpolation of these results (fine estimation). Then, a new complex exponential $v[n]$ is generated

$$v[n] = e^{j\hat{\omega}_i' n} \tag{16}$$

where $\hat{\omega}_i' = 2\pi \hat{f}_i'/f_s$. By means of the matched filter

$$\hat{h} = \frac{1}{N} \sum_{n=1}^{N_{\mathrm{FFT}}} v^*[n] \cdot r[n] \tag{17}$$

the amplitude $\hat{A}_i' = |\hat{h}|$ and the phase $\hat{\phi}_i' = \arg(\hat{h})$ are estimated. Once an exponential is detected, its contribution is subtracted from the initial spectrum, and the procedure starts again. A key point of the IWPA method is that, each time a new frequency is estimated, all previously computed frequencies, amplitudes, and phases are reestimated.

From the quotient among the estimated amplitudes $\hat{A}_i'$ and the transmitted ones A_i, the frequency response of the channel $H(f)$ is estimated. It is important to notice the advantages that this frequency estimation offers when dealing with frequency offsets. These issues are derived from a LO mismatch between the transmitter and the receiver. The IWPA, since it is able to detect the higher received peaks, is able to correctly detect exponentials as well as to calculate the frequency offset.

B. Extension to MIMO Channels

Once the SIMO channel is characterized, the next step involves dealing with a MIMO scheme. This issue can be solved by multiplexing the transmissions along with developing a transmitter identification technique.

1) Multiplexing Technique: This procedure is based on the idea of sequential sounding, following a semiswitched strategy. An orthogonal transmission must be carried out in order to identify each transmit antenna at the receiver nodes. Regarding this issue, two schemes have been studied: a frequency-orthogonal transmission technique and a time-orthogonal transmission technique [15]. The former involves that each transmit antenna uses its own orthogonal set of frequencies to transmit the probe signal. The latter alternates the transmission of $s[n]$ and zeros in order to produce orthogonal transmissions in time. The time-orthogonal alternative has been finally developed due to its simplicity.

2) Transmitter Identification: Considering n_T as the number of transmit antennas, the strategy carried out to identify each one is based on prepending n_T small guard intervals τ_s before each antenna transmission, being the last one $\tau_l > \tau_s$.

At the receiver, we must ensure the presence of n_T complete data blocks in the received signal $r[n]$. The energy signal $e[n]$ is built from the sum of the energy of each received signal $r_a[n]$ by the n_R receive antennas

$$e[n] = \sum_{a=1}^{n_R} |r_a[n]|^2 . \tag{18}$$

To detect the energy, the signal $e[n]$ is fed into a moving-average filter of L_m equal coefficients

$$e_m[n] = e[n] * h_m[n] \quad \text{where} \quad h_m = \begin{cases} 1, & 0 \le n \le L_m - 1 \\ 0, & \text{otherwise.} \end{cases} \tag{19}$$

We can now locate the center of the largest guard interval by correlating the energy with a pulse of length τ_l. Once we have identified it, by knowing the transmission order, we can correctly label the transmissions.

IV. Description of the 4 × 4 MIMO Platform

A typical MIMO test bed includes a transmitter node and a receiver node, each including multiple antennas connected to an analog front end (AFE) which performs the up/down conversion to the BB or intermediate frequency. These platforms and test beds are essential tools to assess, in realistic scenarios, the performance of MIMO systems and algorithms. Moreover, they support real-time transmissions over the air and thus allow for experimenting with true physical channels. Setting up a test bed requires considerable effort, but in many cases, this may still be more economical than, e.g., buying an extremely expensive and less flexible channel sounder which is just intended for measuring.

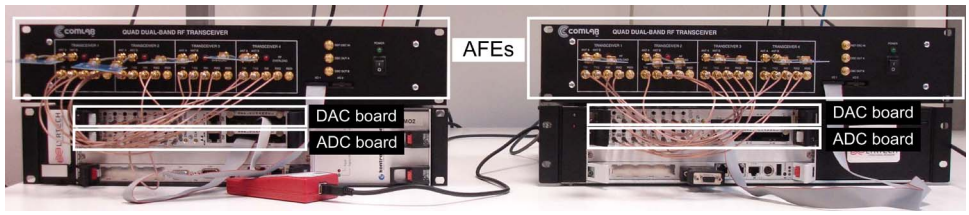

Fig. 3. Two nodes of the 4 × 4 MIMO test bed.

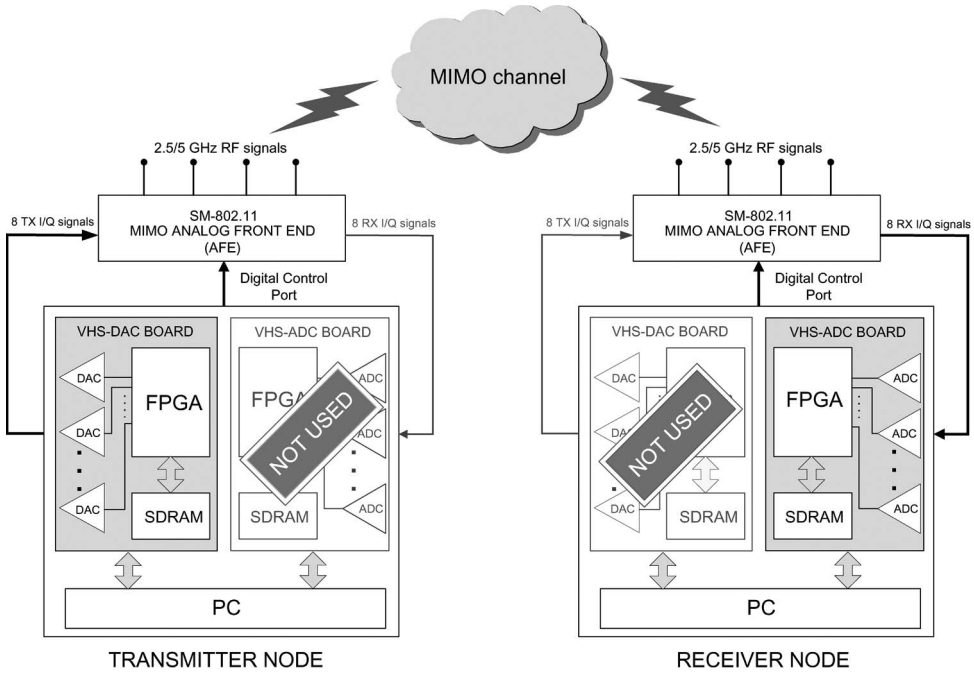

Fig. 4. Block diagram of the 4 × 4 MIMO test bed. (Left) Transmitter node only using DAC board. (Right) Receiver node only using ADC board.

In Fig. 3, we show our dual-band (2.4/5 GHz) MIMO test bed that is capable of targeting both the 2.4- and 5-GHz industrial, scientific, and medical (ISM) bands, being able to transmit and receive complex BB data samples on up to 4 × 4 antennas. It is intended for wideband applications, such as orthogonal frequency-division multiplexing (OFDM), supporting up to a 40-MHz channel bandwidth. Based on the modules by Lyrtech Inc. [34], it consists of two nodes, each one including a PC, a digital-to-analog converter (DAC) board, an analog-to-digital converter (ADC) board, and an AFE. Fig. 4 shows the test-bed block diagram, including the suitable transmitter and receiver setup for performing the measurements.

This testing equipment makes use of FPGA technology for the fast processing of the BB signals. The FPGA in the transmit side is interfaced with a DAC board made up of eight 14-b DACs. The FPGA at the receiver is interfaced with an ADC board made up of eight 14-b ADCs. This real-time signal processing technology is not needed in order to implement this channel characterization methodology. The test bed is able to sample simultaneously eight channels at 26 megasamples per second.

The AFE consists of four independent receive/transmit channels with an output power of 25 dBm at the 1-dB compression point. It is entirely based on the MAX2829 single-chip RF transceiver [35], which has been designed specifically for OFDM 802.11 WLAN applications. The MAX2829 integrates all the circuitry required to implement the RF transceiver function, providing fully integrated receive path, transmit path, voltage-controlled oscillator, frequency synthesizer, and baseband/control serial interface. The AFE is also equipped with four dual-band SkyCross printed antennas [36]. These are suitable for 802.11b/g (from 2.4 to 2.5 GHz) and 802.11a (from 4.9 to 5.85 GHz) applications. They have linear polarization, and the pattern is omnidirectional.

The remote control software based on Web services has been developed in order to handle the test bed [37]. This remote control offers an interface to access all basic functionalities, such as programming the FPGA, adjusting the Transmit/Receive (Tx/Rx) gains, sampling frequencies, etc., and can be accessed and tested through the link http://www.gtas.dicom.unican.es/testbed/ as well as the proposed MIMO channel characterization software.

V. Measurements

Once we have described the methodology (see Section III) and the hardware in which it has been implemented (see Section IV), the first step regarding the measurements leads us to calibrate the complete system as well as validate its proper behavior (see Section V-A). Subsequently, in order to illustrate the proposed methodology performance, a measurement campaign has been performed in an indoor environment (see Section V-C). The MIMO channel frequency response $H(f)$ is

TABLE I
COMPARISON OF CHANNEL SOUNDERS: THE ONE THAT WE ARE PROPOSING IN THIS PAPER (GTAS), THE ONE DEVELOPED AT HELSINKI UNIVERSITY OF TECHNOLOGY (HUT), THE MEDAV RUSK, AND THE ONE DEVELOPED AT DURHAM UNIVERSITY (DURHAM)

	GTAS	HUT	MEDAV RUSK	Durham
RF Frequency (GHz)	2.4, 5	2.145, 5.3	1.8-2.5, 5-6	1.9, 2.1
Maximum antenna matrix ($n_R \times n_T$)	4x4	32x32	8x8	8x8
Multiplexing scheme	Semi-switched	Fully-switched	Fully-switched	Semi-switched
Excitation signal	Multitone CW	PRNS	Multitone CW	Chirp waveform
Synchronization	Not needed	Rubidium	Rubidium	Rubidium
SISO channel measurement time, T_{SISO} (μs)	24.6	8.5	6.4	78
Doppler bandwidth (Hz)[1]	10163	115	2441	1602
Max. scatterers velocity (Km/h)	45	57.9	60	56.84
Bandwidth (MHz)	20	100	120	300
Time delay resolution (ns)	50	10	8.3	3.33

obtained, and the wideband parameters are extracted. A quasi-static channel is assumed such that it remains approximately time invariant within each transmission.

For performing all these measurements, we have considered a 5.33-GHz carrier frequency and a bandwidth $BW = 20$ MHz. The frequency separation between two consecutive exponentials is $\Delta f \approx 1$ MHz, and we consider a sampling frequency $f_s = 26$ MHz and an $N_{\mathrm{FFT}} = 128$ DFT points. In fact, the procedure described in Section III-A1 outputs $M = 20$ exponentials which are separated by $\Delta f' \approx 1.015$ MHz. That means that the covered bandwidth extends from -9.95 to 9.34 MHz around the carrier frequency.

Moreover, a performance comparison between different channel sounders and the one that we are referring to is summarized in Table I. This table presents a comparison between the channel sounding system proposed in this paper and the other current approaches for measuring the MIMO channel. As can be expected, these sounders outperfom ours by achieving a higher measured bandwidth (a better time resolution), a better frequency resolution, and a higher storage capacity. However, the use of a MIMO test bed to implement the proposed methodology involves a cheaper solution aside from reducing the complexity since synchronization between nodes is not needed.

A. System Validation

Prior to the measurements, a back-to-back calibration has been carried out in order to compensate the Tx/Rx frequency responses of the test bed AFE and BB chains. Each Tx/Rx antenna combination has been connected by means of a cable and a 35-dB attenuator. This represents the minimum allowable value for avoiding receiver saturation. In a free-space environment (according to the Friis formula, the loss exponent is equal to two), it represents about 25 cm.

We have considered an attenuation of 35 dB as the mean value returned by 1000 executions of the IWPA algorithm when transmitting a power of -7 dBm. The 95% bootstrap confidence interval for that mean is 0.37 dB. Regarding the FFT algorithm, these values were 36.71 and 0.74 dB, respectively. The linear estimated amplitude of the data is assumed to be Gaussian distributed.

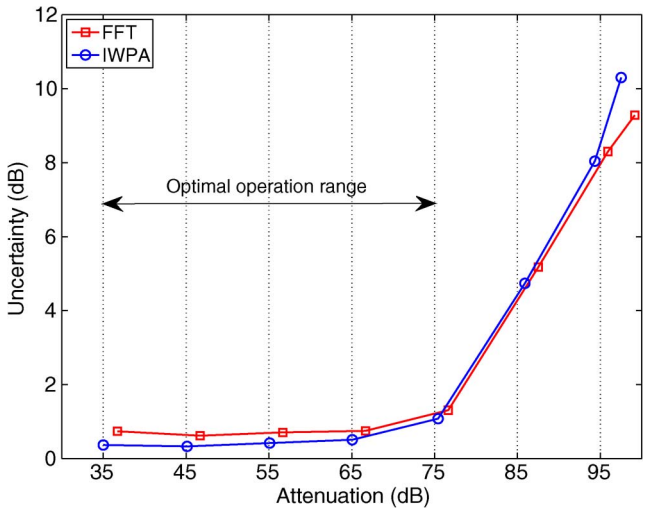

Fig. 5. Precision and operating range of the estimation methods used at the receiver: FFT and IWPA.

These results have been carried out when the transmitter and the receiver are placed 1, 5, and 10 m apart. Since the same precision has been obtained for the considered distances, we can state that the power reaching the receiver due to spurious radiation does not dominate over the power transmitted through the cable.

1) Precision: To evaluate the system precision, we have varied the attenuation from 35 to 105 dB (in steps of 10 dB), emulating different distances between the transmitter and the receiver (from 25 cm to 800 m). This experiment allows to compare the precision of both algorithms (FFT and IWPA) under different SNR conditions. Moreover, this evaluation is useful for determining their optimal operating ranges. The experiment results are depicted in Fig. 5.

As can be seen, uncertainty noticeably grows up beyond 75 dB (equivalent to 25 m of separation). That means that the optimal operation range covers from 35 to 75 dB of attenuation. Increasing the transmitted power shifts both curves to the right, which means that the operating range enlarges the same quantity (e.g., an additional 16 dB, from 35 to 91 dB, can be obtained by changing the transmitted power from -7 to 9.6 dBm). In summary, the overall range in meters varies from 0.25 to 250.

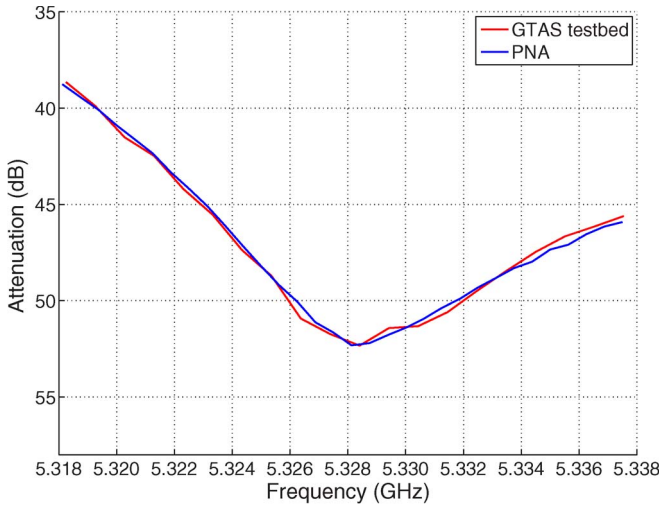

Fig. 6. Comparison of the S_{21} parameter using our technique and the results from the PNA.

Fig. 5 also justifies the use of the IWPA since it outperforms the FFT in terms of uncertainty within the optimal operation range.

2) Accuracy: In order to show how realistic the results are, we have measured a passive filter (one example of a wired single-input single-output (SISO) channel). We have compared our results with those obtained by an Agilent N3383A programmable network analyzer (PNA) with a frequency range from 300 kHz to 9 GHz.

Since the PNA has been thoroughly calibrated, we consider its results as a reference. We have chosen a 20-MHz representative window of the S_{21} filter parameter (forward transmission). This window is centered at $f_{\mathrm{RF}} = 5.328$ GHz. Subsequently, at the same RF, we have measured the filter response with our system.

Both measurements are depicted in Fig. 6, and the obtained results show that the proposed measurement system accurately reflects the reality. Since the measurement systems were calibrated, the vertical axis represents the attenuation (in decibels) introduced by the filter.

B. Description of Measurement Scenarios

Fig. 7 shows the layout of the measurement site in the laboratory of the Advanced Signal Processing Group (GTAS) at the University of Cantabria. The laboratory is furnished with office equipment: tables, PCs, and seats. To obtain the wideband MIMO channel parameters, we conducted a series of measurements according to the transmit and receive node locations. Three scenarios are analyzed, keeping fixed the receiver (RX in Fig. 7). The transmitter in the first experiment (TX 1 in Fig. 7) is placed 3.5 m away from the receiver, with a clear line of sight (LOS) between them. In the second experiment, the transmitter (TX 2 in Fig. 7) was located further away from the receiver ($\approx$12 m), avoiding a clear LOS. In the third experiment, the transmitter (TX 3 in Fig. 7) was not placed in the laboratory but in the middle of the corridor. The transmitted power ranges from -7 to 9.6 dBm, depending on the transmitter location.

Two different environments have been considered, depending on the mobility. In a low-mobility environment, the transmitter is kept fixed at each location during each experiment. In the second environment, the measures are taken by moving the transmitter within a small local area (e.g., 900 cm^2) among the experiments, but the transmitter is kept still during the experiments so that no Doppler effect exists due to movement. This is usually referred to as a nomadic scenario, whose aim is to obtain a statistical analysis by averaging the obtained measures in space.

C. Experimental Results

A series of measurements has been carried out considering the three transmitter locations and the different mobility environments. These measurements have been performed, making use of a MATLAB GUI tool, which has also been developed to easily collect the data.

Fig. 8 represents the transmission diagram of our semi-switched system for a 4×4 configuration. The signal $s[n]$ transmitted with transmit antenna 1 is denoted as $s_1[n]$, as $s_2[n]$ with transmit antenna 2, and so on. Since we use parallel receivers, the time that a SISO measurement takes T_{SISO} matches up with the time for estimating a SIMO channel T_{SIMO}. The time required for a MIMO measurement is denoted as T_{snapshot}. The spaces among transmissions that allow for transmitter identification are denoted as τ_s and τ_l.

Bearing in mind that a cyclic transmission is carried out, this tool allows the user to set the time between measurements (or channel snapshots) T_{meas} as well as the number of measurements. Concretely, our system allows MIMO channel snapshots to be estimated consecutively, i.e., $T_{\mathrm{meas}} = T_{\mathrm{snapshot}}$, or introduces "no transmission" gaps among snapshots τ_{sleep}, which means that the time between the measurements will be $T_{\mathrm{meas}} = T_{\mathrm{snapshot}} + \tau_{\mathrm{sleep}}$.

Low-mobility measurements have been performed to study the time variability of the channel at the different transmitter node locations. As an example, the MIMO channel frequency response at position 1 is depicted in Fig. 9, considering that $T_{\mathrm{meas}} = 100$ ms and $\tau_{\mathrm{sleep}} \approx T_{\mathrm{meas}} - n_T \cdot T_{\mathrm{SISO}} = 100$ ms $- 4 \cdot 24.6$ μs $= 99.9$ ms; hence, the 11 curves represent each SISO channel. These 11 curves are almost perfectly overlapping and cannot be individually resolved in the presented graphs.

1) Wideband Parameter Estimation: Let us consider a nomadic environment in order to obtain wideband parameters: coherence bandwidth B_c and delay spread σ_τ. The three transmitter locations are considered to make the wideband parameter comparisons by varying certain parameters, such as the transmitting and receiving node separation, object reflections, LOS/non-LOS conditions, etc.

In a general manner, from $H(f)$, we can obtain the normalized autocorrelation function R_H as

$$R_H(f, f + \Delta f) = E\left[H^*(f)H(f + \Delta f)\right] = R_H(\Delta f). \quad (20)$$

Then, from R_H, we can graphically obtain B_c as depicted in Fig. 10, considering the fact that B_c is equal to the frequency difference where the normalized autocorrelation value is 0.5.

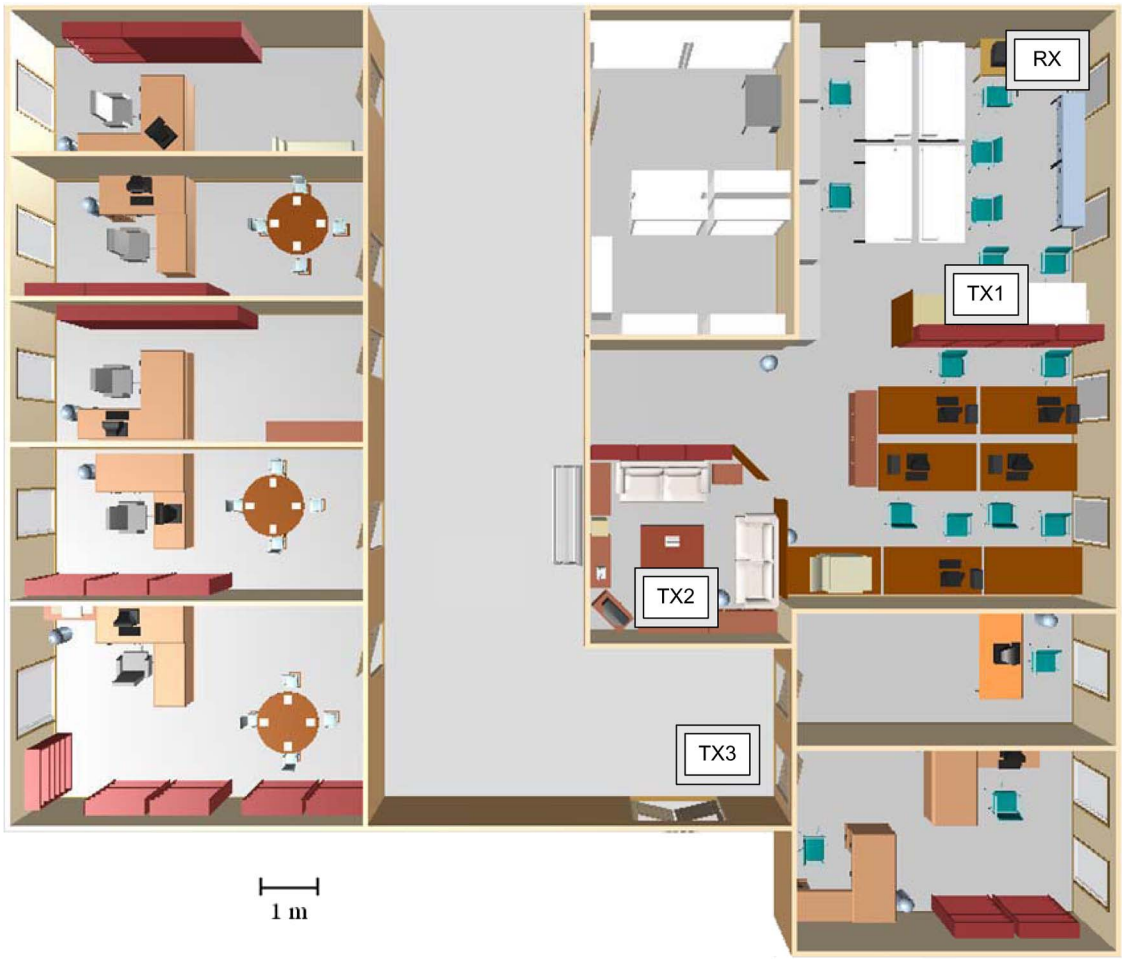

Fig. 7. Node locations of the different experiments conducted at the laboratory of the GTAS.

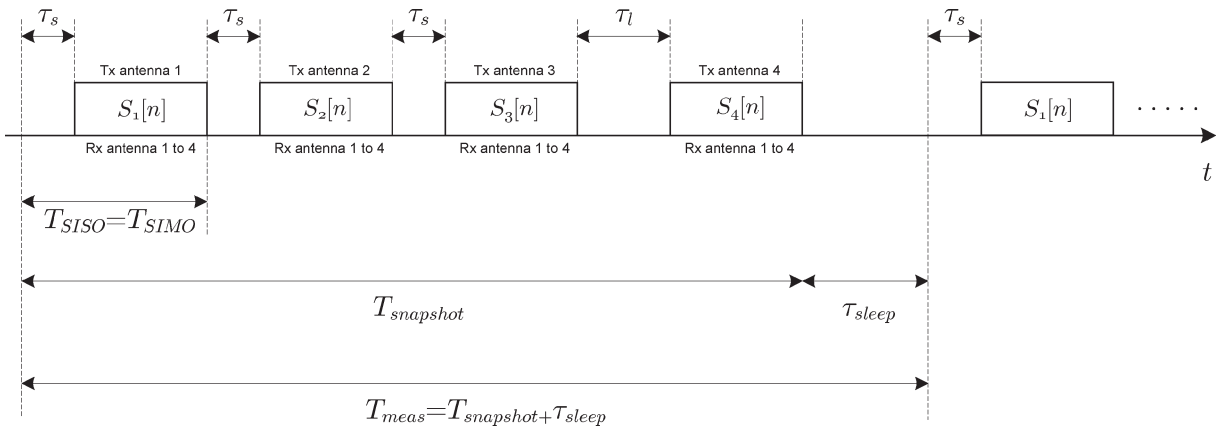

Fig. 8. Time diagram representing the transmission/reception scheme for our 4 × 4 antenna configuration.

The rule of thumb to obtain the rms delay spread in this case is given by [38]

$$\sigma_\tau = \frac{0.2}{B_c}. \tag{21}$$

In Table II, a summary of the obtained wideband parameters in a nomadic environment is shown. The coherence bandwidth and delay spreads have been obtained by averaging the results of up to 1000 snapshots and all the 16 SISO channels. As was expected and according to these averaged results, the coherence bandwidth was observed to decrease as the transmitter moves away with respect to the receiver. However, the decrease trend is not monotonic since the coherence bandwidth is highly fluctuating due to the multipath.

VI. Conclusion

In this paper, the design and implementation of a flexible broadband MIMO channel measurement methodology have

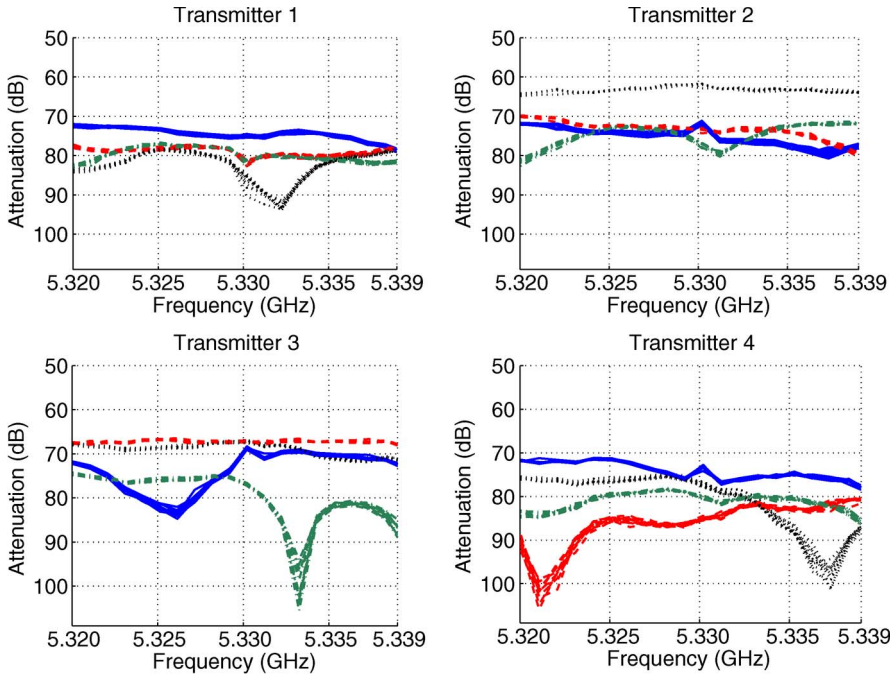

Fig. 9. MIMO channel frequency response measured at position 1 in a low-mobility environment. The 11 curves for each SISO channel are represented.

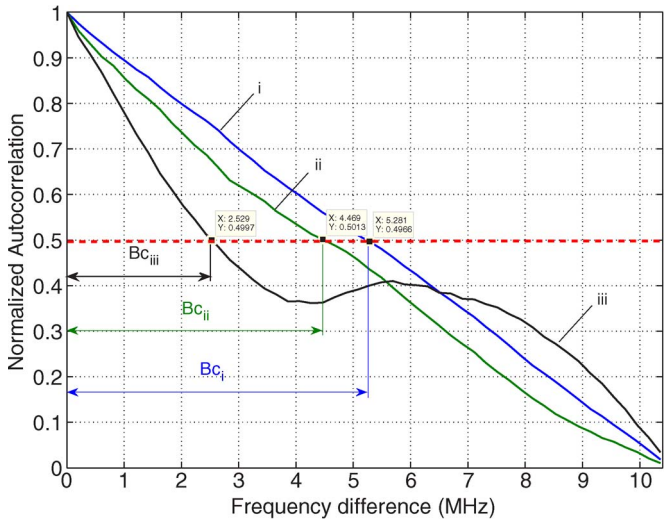

Fig. 10. Example of coherence bandwidth calculation from the normalized autocorrelation function for different channels. (i) Non-frequency-selective channel. (ii) Intermediate channel. (iii) Frequency-selective channel.

TABLE II
WIDEBAND PARAMETERS

Transmitter Position	Coherence bandwidth (MHz)	Delay spread (ns)
TX1	9.185	22.736
TX2	8.275	26.207
TX3	7.796	28.165

been presented. Unlike other channel characterization systems, it is able to be implemented in any transmit/receive hardware without needing either additional synchronization circuitry or real-time processing. The methodology has been implemented over a 4×4 dual-band (2.4/5 GHz) MIMO test bed. Obtained measures and wideband parameters in several locations are shown and analyzed. The resulting MIMO channel matrices can be stored and used in link-level simulations of communications systems in order to obtain results that are representative of real-world situations.

REFERENCES

[1] G. Foschini and M. Gans, "On limits of wireless communications in a fading environment when using multiple antennas," *Wireless Pers. Commun.*, vol. 6, no. 3, pp. 311–335, Mar. 1998.
[2] I. E. Telatar, "Capacity of multi-antenna Gaussian channels," *Eur. Trans. Telecommun.*, vol. 10, no. 6, pp. 585–595, Nov./Dec. 1999.
[3] M. K. Simon and M.-S. Alouini, *Digital Communications Over Fading Channels*, J. G. Proakis, Ed. New York: Wiley, 2005.
[4] 3GPP—3GPP2 Spatial Channel Model Ad-hoc Group, *Spatial Channel Model for Multiple Input Multiple Output (MIMO) Simulations*, 3GPP TR 25.996 v6.1.0, Sep. 2003.
[5] L. M. Correia, *Mobile Broadband Multimedia Networks: Techniques, Models and Tools for 4G*. New York: Academic, 2006.
[6] [Online]. Available: https://www.ist-winner.org
[7] *Winner II Interim Channel Models*, IST-4-027756 WINNER II D.1.1.1, Dec. 2006.
[8] R. S. Thomä, M. Landmann, A. Richter, and U. Trautwein, "Multidimensional high-resolution channel sounding measurement," in *Smart Antennas State of the Art*, T. Kaiser, A. Bourdoux, H. Boche, J. R. Fonollosa, and J. B. Andersen, Eds. New York: Hindawi Publishing Corp., 2005, pp. 241–270.
[9] K. Sakaguchi, J. Takada, and K. Araki, "A novel architecture for MIMO spatio-temporal channel sounder," *IEICE Trans. Electron.*, vol. E85-C, no. 3, pp. 436–441, 2002.
[10] I. Santamaría, C. Pantaleón, and J. Ibáñez, "A comparative study of high-accuracy frequency estimation methods," *Mech. Syst. Signal Process.*, vol. 14, no. 5, pp. 819–834, Sep. 2000.
[11] [Online]. Available: http://www.channelsounder.de
[12] J. Kivinen, T. O. Korhonen, P. Aikio, R. Gruber, and P. Vainikainen, "Wideband radio channel measurement system at 2 GHz," *IEEE Trans. Instrum. Meas.*, vol. 48, no. 1, pp. 39–44, Feb. 1999.
[13] B. T. Maharaj, J. W. Wallace, M. A. Jensen, and L. P. Linde, "A low-cost open-hardware wideband multiple-input-multiple-output (MIMO) wireless channel sounder," *IEEE Trans. Instrum. Meas.*, vol. 57, no. 10, pp. 2283–2289, Oct. 2008.
[14] S. J. Howard and K. Pahlavan, "Measurement and analysis of the indoor radio channel in the frequency domain," *IEEE Trans. Instrum. Meas.*, vol. 39, no. 5, pp. 751–755, Oct. 1990.

[15] J.-M. Molina-Garcia-Pardo, J.-V. Rodriguez, and L. Juan-Llacer, "MIMO channel sounder based on two network analyzers," *IEEE Trans. Instrum. Meas.*, vol. 57, no. 9, pp. 2052–2058, Sep. 2008.
[16] A. G. i. Fábregas, M. Guillaud, D. T. M. Slock, G. Caire, K. Gosse, S. Rouquette, A. R. Dias, P. Bernardin, X. Miet, J.-M. Conrat, Y. Toutain, A. Peden, and Z. Li, "A MIMO-OFDM testbed for wireless local area networks," *EURASIP J. Appl. Signal Process.*, vol. 2006, p. 135, Jan. 2010.
[17] S. Caban, C. Mehlführer, R. Langwieser, A. L. Scholtz, and M. Rupp, "Vienna MIMO testbed," *EURASIP J. Appl. Signal Process.—Special Issue on Implementation Aspects and Testbeds for MIMO systems*, vol. 2006, p. 142, Jan. 2006.
[18] D. Ramírez, I. Santamaría, J. Pérez, J. Vía, J. A. García-Naya, T. M. Fernández-Caramés, H. Pérez-Iglesias, M. G. López, L. Castedo, and J. M. Torres-Royo, "A comparative study of STBC transmissions at 2.4 GHz over indoor channels using a 2×2 MIMO testbed," *Wireless Commun. Mobile Comput.*, vol. 8, no. 9, pp. 1149–1164, Nov. 2008.
[19] D. Baum, D. Gore, R. Nabar, S. Panchanathan, K. Hari, V. Erceg, and A. Paulraj, "Measurement and characterization of broadband MIMO fixed wireless channels at 2.5 GHz," in *Proc. IEEE Int. Conf. Pers. Wireless Commun.*, 2000, pp. 203–206.
[20] J. Kivinen, X. Zhao, and P. Vainikainen, "Empirical characterization of wideband indoor radio channel at 5.3 GHz," *IEEE Trans. Antennas Propag.*, vol. 49, no. 8, pp. 1192–1203, Aug. 2001.
[21] J. Peigang, W. Shaobo, and L. Huajia, "An effective solution of wireless channel sounder and its channel modeling application," in *Proc. Veh. Technol. Conf.*, May 2004, vol. 1, pp. 249–253.
[22] J. D. Parsons, *The Mobile Radio Propagation Channel*. New York: Wiley, 2000.
[23] A. H. Kemp and E. B. Bryant, "Channel sounding of industrial sites in the 2.4 GHz ISM band," *Wireless Pers. Commun.*, vol. 31, no. 3/4, pp. 235–248, Dec. 2004.
[24] H. K. Chung, N. Vloeberghs, H. K. Kwon, S. J. Lee, and K. C. Lee, "MIMO channel sounder implementation and effects of sounder impairment on statistics of multipath delay spread," in *Proc. Veh. Technol. Conf.*, Sep. 2005, vol. 1, pp. 349–353.
[25] S. Salous and N. Razavi-Ghods, *Semi-Sequential MIMO Channel Measurements in Indoor Environments*, Gothenburg, Sweden, COAT 273 TD(04) 079, Jun. 2004.
[26] R. Thoma, D. Hampicke, A. Richter, G. Sommerkorn, A. Schneider, U. Trautwein, and W. Wirnitzer, "Identification of time-variant directional mobile radio channels," *IEEE Trans. Instrum. Meas.*, vol. 49, no. 2, pp. 357–364, Apr. 2000.
[27] B. Maharaj, L. Linde, J. Wallace, and M. Jensen, "A cost-effective wideband MIMO channel sounder and initial co-located 2.4 GHz and 5.2 GHz measurements," in *Proc. IEEE ICASSP*, Mar. 2005, vol. 3, pp. iii/981–iii/984.
[28] W. Wirnitzer, D. Bruckner, R. Thoma, G. Sommerkorn, and D. Hampicke, "Broadband vector channel sounder for MIMO channel measurement," in *Proc. IEE Seminar MIMO—Communications Systems From Concept to Implementations (Ref. No. 2001/175)*, Dec. 2001, pp. 17/1–17/4.
[29] S. Salous, P. Filippidis, R. Lewenz, I. Hawkins, N. Razavi-Ghods, and M. Abdallah, "Parallel receiver channel sounder for spatial and MIMO characterisation of the mobile radio channel," *Proc. Inst. Elect. Eng.—Commun.*, vol. 152, no. 6, pp. 912–918, Dec. 2005.
[30] J. Takada, K. Sakaguchi, and K. Araki, "Development of high resolution MIMO channel sounder for the advanced modeling of wireless channels," in *Proc. APMC*, Dec. 2001, vol. 2, pp. 563–568.
[31] J. Tubbax, B. Côme, L. V. der Perre, S. Donnay, M. Moonen, and H. D. Man, "Compensation of transmitter IQ imbalance for OFDM systems," in *Proc. IEEE ICASSP*, 2004, pp. ii-325–ii-328.
[32] E. V. der Ouderaa, J. Schoukens, and J. Renneboog, "Peak factor minimization using a time-frequency domain swapping algorithm," *IEEE Trans. Instrum. Meas.*, vol. 37, no. 1, pp. 145–147, Mar. 1988.
[33] S. Boyd, "Multitone signals with low crest factor," *IEEE Trans. Circuits Syst.*, vol. CAS-33, no. 10, pp. 1018–1022, Oct. 1986.
[34] [Online]. Available: http://www.lyrtech.com/
[35] [Online]. Available: http://datasheets.maxim-ic.com/en/ds/MAX2828-MAX2829.pdf
[36] [Online]. Available: http://www.skycross.com/Products/wireless.html
[37] L. Vielva, J. Vía, J. Gutiérrez, O. González, J. Ibáñez, and I. Santamaría, "Building a web platform for learning advanced digital communications using a MIMO testbed," in *Proc. IEEE ICASSP*, Mar. 2010, pp. 2942–2945.
[38] G. Durgin, "Random fading channels," in *Space-Time Wireless Channels*. Englewood Cliffs, NJ: Prentice-Hall, 2002.

Jesús Gutiérrez (S'08) received the B.S. degree in telecommunication engineering from the University of Cantabria, Santander, Spain, in 2008, where he has been working toward the Ph.D. degree in the Communications Engineering Department, under the supervision of J. Ibáñez and J. Pérez, since 2008.

His current research interests include signal processing for wireless communications, multiple-input multiple-output (MIMO) systems, and MIMO test beds. He has been involved in several national and international research projects on these topics.

Óscar González (S'10) received the B.S. degree in telecommunication engineering from the University of Cantabria, Santander, Spain, in 2009, where he has been working toward the Ph.D. degree in the Communications Engineering Department, under the supervision of I. Santamaría, since 2009.

His current research interests include signal processing for wireless communications, multiple-input multiple-output (MIMO) systems, MIMO test beds, and interference alignment.

Jesús Pérez (M'01) received the M.S. and Ph.D. degrees in applied physics from the University of Cantabria, Santander, Spain.

In 1989, he was with the Radiocommunication and Signal Processing Department, Polytechnic University of Madrid, Madrid, Spain, as a Junior Researcher. From 1990 to 1998, he was with the Electronics Department, University of Cantabria, as a Ph.D. student and, later, as an Associate Professor. In 1998, he was with the University of Alcalá, Madrid, Spain, as an Assistant Professor. From 2000 to 2003, he was with T.T.I. Norte as a Senior Engineer. Since 2003, he has been a Senior Researcher with the Communications Engineering Department, University of Cantabria, where he is currently an Associate Professor. His main research interests include signal processing, with a focus on wireless communications.

David Ramírez (S'07) received the B.S. degree in telecommunication engineering from the University of Cantabria, Santander, Spain, in 2006, where he has been working toward the Ph.D. degree in the Communications Engineering Department, under the supervision of I. Santamaría and J. Vía, since 2006.

He has been a Visiting Researcher, under the supervision of Prof. Peter J. Schreier, at The University of Newcastle, Newcastle, Australia. His current research interests include signal processing for wireless communications, multiple-input multiple-output (MIMO) systems, MIMO test beds, cognitive radio, and multivariate statistical analysis. He has been involved in several national and international research projects on these topics.

Luis Vielva was born in Santander, Spain, in 1966. He received the Licenciado and Ph.D. degrees in physics from the University of Cantabria, Santander, Spain.

Since 1989, he has been with the Communications Engineering Department, University of Cantabria, where he is currently an Associate Professor. His current research interests include systems biology, convex optimization, and geometric algebra.

Jesús Ibáñez (S'00–M'05) was born in Santander, Spain, in 1971. He received the B.S. degree in telecommunication engineering and the Ph.D. degree from the University of Cantabria, Santander, Spain, in 1995 and 2004, respectively.

Since 1995, he has been with the Communications Engineering Department, University of Cantabria, where he is currently an Associate Professor. His research interests include digital signal processing and digital communication applied to multiple-input multiple-output systems and sensor networks.

Ignacio Santamaría (M'96–SM'05) received the B.S. degree in telecommunication engineering and the Ph.D. degree in electrical engineering from the Universidad Politécnica de Madrid, Madrid, Spain, in 1991 and 1995, respectively.

Since 1992, he has been with the Communications Engineering Department, University of Cantabria, Santander, Spain, where he is currently a Full Professor. He has been a Visiting Researcher at the Computational NeuroEngineering Laboratory, University of Florida, Gainesville, and at the Wireless Networking and Communications Group, University of Texas at Austin, Austin. He has more than 100 publications in refereed journals and international conference papers. His current research interests include signal processing algorithms for wireless communication systems, multiple-input multiple-output systems, multivariate statistical techniques, and machine learning theories. He has been involved in several national and international research projects on these topics.

Dr. Santamaría is currently a member of the Machine Learning for Signal Processing Technical Committee of the IEEE Signal Processing Society.